

Fig. 2. (A) SDS-PAGE analysis of intact rhFS (lane 1) and PNGaseF-digested rhFS (lane 2). Lane M represents molecular weight markers. (B) IEF of intact rhFS (lane 1) and neuraminidase-digested rhFS (lane 2). Lane M represents *pI* markers.

the non-glycosylated FS and the glycosylated FS with diverse N-linked oligosaccharides, respectively.

The sialic acid heterogeneity of rhFS was analyzed by IEF with and without neuraminidase digestion. IEF of intact rhFS showed that the majority of the isoforms are located from *pI* 6.9 to 7.4 (Fig. 2B, lane 1). After treatment with neuraminidase, the acidic bands had disappeared and shifted at *pI* 7.4 (Fig. 2B, lane 2). These results suggested that the sialic acids contribute to the heterogeneity and the charge of rhFS.

The distribution of glycoforms was further investigated by MALDI-TOF MS. As shown in Fig. 3, multiple ions were detected in the range of 31.5–37 kDa. The most abundant ion at *m/z* 31,525 corresponded to the theoretical mass of non-glycosylated FS (31,514 Da). The other ions at *m/z* 33,804 and 35,600 could have

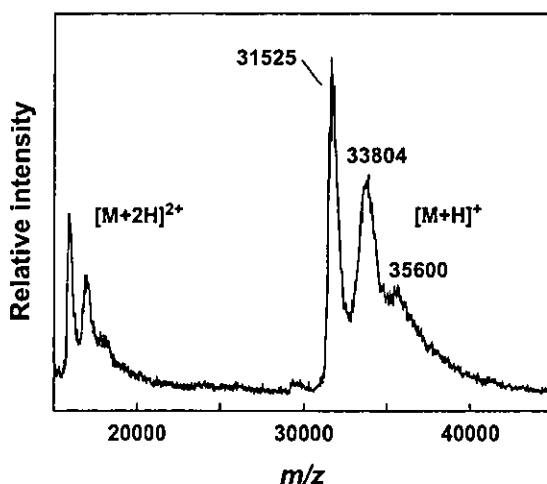


Fig. 3. MALDI-TOF MS analysis of intact rhFS. The peaks at *m/z* 31,525, 33,804 and 35,600 correspond to the non-glycosylated and glycosylated form of rhFS, respectively.

been monoglycosylated FS and diglycosylated FS, respectively.

3.2. Monosaccharide composition of rhFS

Monosaccharide composition was analyzed by hydrolysis followed by HPAEC-PAD. The relative molecular ratio of fucose and glucosamine were estimated at 1.2 and 4.4, respectively, when mannose was considered as 3.0 (Table 1). This result suggests the presence of fucosylated bi- and triantennary-type oligosaccharides. No galactosamine residue was detected, suggesting the absence of O-linked oligosaccharides.

3.3. N-linked oligosaccharides in rhFS

N-linked oligosaccharides were released from rhFS by PNGaseF digestion and reduced with NaBH_4 to avoid the separation of anomers. Then the oligosaccharide alditols from rhFS were analyzed by GCC-LC/MS. Fig. 4 shows the total ion current chromatogram of N-linked oligosaccharide alditols. The *m/z* values of intense ions observed in major peaks (peaks 8 and 12) were 1040.7^{2+} and 1186.4^{2+} , which were consistent with the theoretical *m/z* values of $[\text{dHex}][\text{Hex}]_5[\text{HexNAc}]_4[\text{NeuAc}]_2^{2+}$ and $[\text{dHex}][\text{Hex}]_5[\text{HexNAc}]_4[\text{NeuAc}]_2^{2+}$, respectively (Table 2). The elution times of these oligosaccharides were in good agreement with those of fucosyl biantennary oligosaccharides bearing mono- and di-NeuAc prepared from erythropoietin, respectively [24]. An ion at *m/z* 1041.4^{2+} was also detected in peak 6. This oligosaccharide could be a sialylation isomer of peak 8 (1040.7^{2+}).

Likewise, the ions at *m/z* 1790.7^+ and 895.4^{2+} in peak 2 and at *m/z* 1077.9^{2+} in peak 3 were assigned as an asialo fucosylated biantennary oligosaccharide and an asialo fucosylated triantennary oligosaccharide, respectively. The ion at *m/z* 2389.6^+ and 1194.6^{2+} in peak 11 was consistent with $[\text{dHex}][\text{Hex}]_5[\text{HexNAc}]_4[\text{NeuAc}][\text{NeuGc}]^{2+}$ or $[\text{Hex}]_6[\text{HexNAc}]_4[\text{NeuAc}]_2^{2+}$, respectively. The ions at *m/z* 2097.7^+ and 1048.6^{2+} in peak 5 and at *m/z* 2096.5^+ and 1049.5^{2+} in peak 8 were consistent with $[\text{dHex}][\text{Hex}]_5[\text{HexNAc}]_4[\text{NeuGc}]^{2+}$ or $[\text{Hex}]_6[\text{HexNAc}]_4[\text{NeuAc}]^{2+}$, respectively. The minor ions at *m/z* 1224.1^{2+} , 1224.3^{2+} , 1369.7^{2+} , 1369.8^{2+} ,

Table 1
Monosaccharide composition analysis of rhFS oligosaccharides

Monosaccharide	Relative molar proportions ^a
Fucose	1.2
Galactosamine	0.3
Glucosamine	4.4
Galactose	3.2
Glucose	0.3
Mannose	3.0

^a Data are normalized to three-mannose residues.

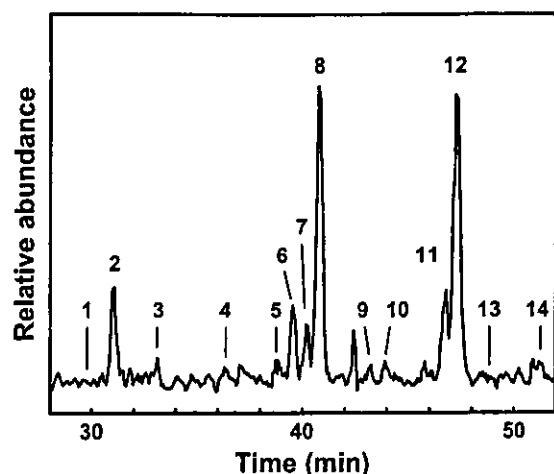


Fig. 4. Sugar map of oligosaccharide alditols released from rhFS. N-linked oligosaccharide alditols from rhFS were separated with GCC. The total ion content was scanned using the positive-ion mode at m/z 700–2400.

1370.5²⁺ and 1515.5²⁺ in peaks 7, 9, 11, 12, 13 and 14 were deduced to the fucosylated triantennary oligosaccharides with NeuAc, respectively.

The ratio of oligosaccharides was estimated as follows: fucosylated biantennary, ca. 85%, and fucosylated triantennary structures, ca. 10%, based on their ion currents; these results were in good agreement with the results of the monosaccharide composition analysis.

3.4. Site-specific glycosylation of rhFS

FS contains two potential *N*-glycosylation sites (Asn95 and Asn259, Fig. 1). The site-specific glycosylation and other post-translational modifications, such as phosphorylation and hydroxylation, were analyzed by mass spectrometric peptide/glycopeptide mapping (Fig. 5a, Table 3). Most of the non-glycosylated peptides were detected except for the small peptides, i.e. peptides D2 (tripeptide), D13 (tetrapeptide), and D12 (pentapeptide), which suggests the absence of *O*-glycans and any post-translational modifications on these peptides. The small peptides have no putative *N*-glycosylation site (Fig. 1), and no galactosamine residue was detected (Table 1). These findings suggest the absence of *N*- and *O*-linked oligosaccharides. However, the possibility remains that the small peptides are modified, such as by phosphorylation. Two unpredicted peptides (m/z 1176.2²⁺ and 510.4²⁺) were detected among the Asp-N digests of rhFS. They were assigned to peptides D15-1 and D15-2, which were produced from peptide D15 by further cleavage at the amino-terminal of Glu280. It was reported that a cleavage at the N-terminal site of glutamic acid is a possible cut site for Asp-N under the same conditions [25]. Peptides D5 and D15-1, each of which

Table 2
Putative structures of N-linked oligosaccharides deduced from the GCC-LC/MS

Peak No. ^a	Carbohydrate structure ^b	Theoretical mass ^c	Observed mass ^d		
			M ⁺	M ²⁺	M ³⁺
1		1627.5	1628.3	814.2	-
2		1789.7	1790.7	895.4	-
3		2155.0	-	1077.9	-
4		1934.7	-	967.9	-
5		2096.9	2097.7	1048.6	-
6		2080.9	2081.2	1041.4	-
7		2446.3	-	1224.1	817.4
8		2096.9	2096.5	1049.6	-
		2080.9	2082.2	1040.7	-
9		2446.3	-	1224.3	-
10		2226.0	-	1114.2	-
11		2388.2	2389.6	1194.6	-
		2737.5	-	1369.7	913.4
12		2372.2	2372.2	1186.4	-
		2737.5	-	1369.8	-
13		2737.5	-	1370.5	913.8
14		3028.8	-	1515.5	-

Note: The observed m/z of *1 and *2 are also consistent with the theoretical m/z value of [Hex]₆[HexNAc]₄[NeuAc] and [Hex]₆[HexNAc]₄[NeuAc]₂, respectively.

^a Peak label in Fig. 4.

^b Proposed structures based on molecular weight. Symbols: solid squares, GlcNAc; open circles, mannose; open diamonds, galactose; dotted diamonds, fucose; solid circle, NeuAc; dotted circle, NeuGc.

^c Calculated average mass.

^d Mass of the ion measured in the positive-ion ESI mass spectrum from alditols.

have potential glycosylation site, were detected as non-glycosylated forms in the peptide/glycopeptide map.

Precursor-ion scanning, which can detect [Hex][HexNAc]⁺ at m/z 366 produced by collision-induced dissociation, was performed for the monitoring of the glycopeptides. The TIC chromatogram of the precursor-ion scanning showed two significant peaks, peaks G1 and G2 (Fig. 5b). Fig. 6 shows the mass spectra of peaks G1 and G2 in Fig. 5b. On the basis of the theoretical masses of the peptides and oligosaccharides identified by sugar mapping (Table 2), peaks G1 and G2

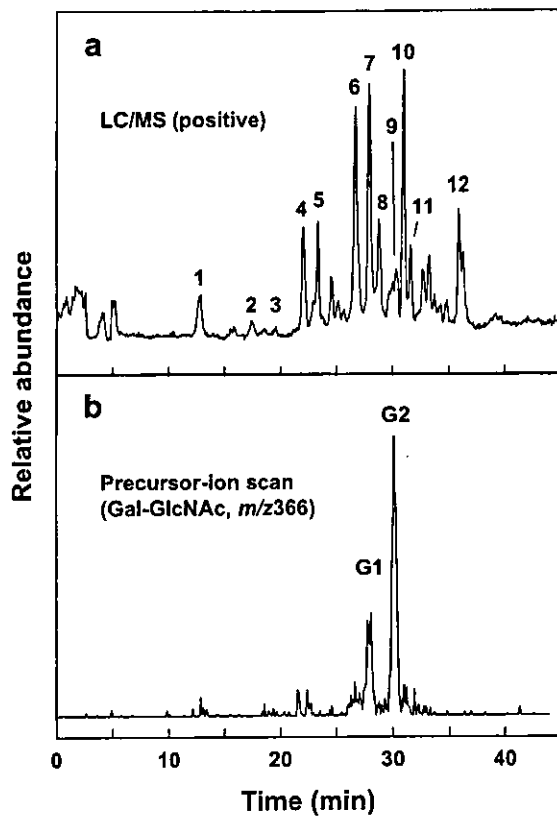


Fig. 5. Peptide/glycopeptide map of the rhFS Asp-N digest. The total ion current chromatogram of LC/MS in the positive-ion mode at m/z 400–2400 (a), and the TIC chromatogram of LC/MS/MS, precursor-ion scan of m/z 366 (b).

were assigned to glycosylated D5 and D15-1, respectively. The oligosaccharides attached to each *N*-glycosylation site were deduced as shown in Table 4. By comparing the *N*-linked oligosaccharide structures on

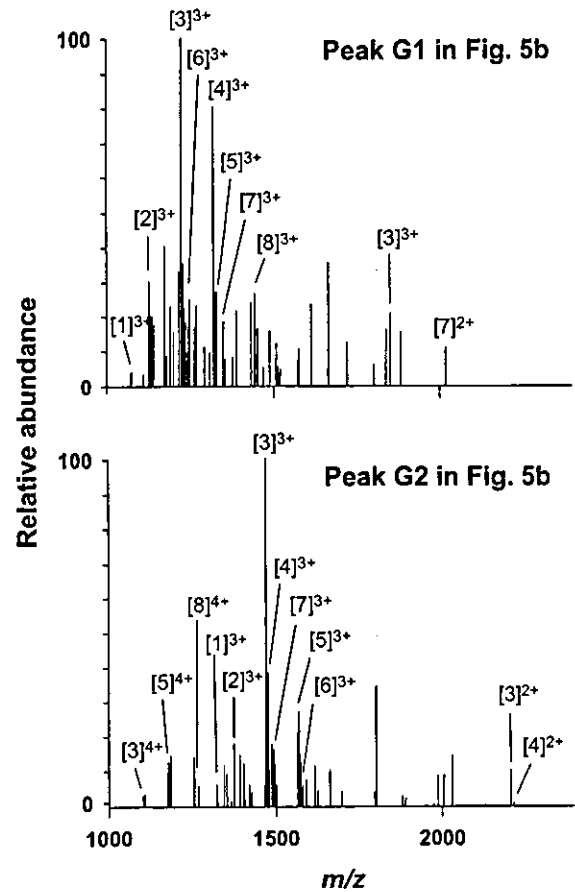


Fig. 6. Mass spectra of glycopeptides in peaks G1 and G2 in Fig. 5b. The observed m/z value of each ion is summarized in Table 4.

Asn95 with those on Asn259, it was concluded that biantennary oligosaccharides are major oligosaccharides located at both Asn95 and Asn259, whereas the triantennary structures are present mainly at Asn95.

Table 3
Assignment of the peaks in Fig. 5a

Peak no. ^a	Peptide ^b	Theoretical mass ^c	Observed m/z ^d					
			M^+	M^{2+}	M^{3+}	M^{4+}	M^{5+}	M^{6+}
1	D4	2666.0	—	1334.2	889.9	667.4	—	—
2	D14	777.8	778.6	—	—	—	—	—
3	D15-2 ^e	1018.0	1019.0	510.4	—	—	—	—
4	D11	1456.6	1457.5	729.0	486.3	—	—	—
5	D6	4378.8	—	—	1460.8	1095.5	—	—
6	D8	3326.4	—	1664.6	1109.5	—	—	—
	D10	1467.6	1468.2	734.8	490.1	—	—	—
7	D1	4728.1	—	—	1577.0	1183.2	947.0	789.6
8	D7	1329.4	1330.2	665.3	—	—	—	—
9	D5	1608.7	1609.3	805.1	—	—	—	—
10	D9	4165.6	—	—	1389.0	1042.2	834.1	—
11	D15-1 ^e	2350.6	—	1176.2	784.2	—	—	—
12	D3	3219.5	—	1610.1	1073.8	806.4	—	—

^a Peak label in Fig. 5a.

^b Predicted peptides were shown in Fig. 1.

^c Calculated average mass.

^d Mass of the ions measured in the positive-ion ESI mass spectrum from precursor-ion scan.

^e Peptide derived from D15 peptide.

4. Discussion

The aim of the present study was to analyze the distribution of the glycoforms and the carbohydrate structures of rhFS. Previous study of FS isolated from porcine ovary has shown that porcine FS exists in six isoforms, due to alternative splicing and the site occupancy of N-linked oligosaccharides [8]. In this study, we used rhFS288 to eliminate the heterogeneity due to alternative splicing. The results of SDS-PAGE and MALDI-TOF MS revealed the presence of both non-glycosylated and glycosylated forms (Figs. 2 and 3). FS contains two potential N-glycosylation sites. Using mass spectrometric peptide/glycopeptide mapping and precursor-ion scanning, we found that both N-glycosylation sites were partially glycosylated (Fig. 5 and Table 3). Non-glycosylated and glycosylated proteins containing Asn95 and Asn259 were detected in the peptide/glycopeptide map and precursor-ion scanning, respectively. Monosaccharide composition analyses suggested the presence of linkages of fucosylated bi- and triantennary complex-type oligosaccharides on rhFS (Table 1). This finding was supported by mass spectrometric oligosaccharide profiling, in which the *m/z* values and

elution times of some of the oligosaccharides from rhFS were in good agreement with those of standard oligosaccharides. The site-specific glycosylations were deduced on the basis of the mass spectra of glycopeptides. It was suggested that biantennary oligosaccharides attach to both Asn95 and Asn259, whereas triantennary oligosaccharides attach mainly to Asn95 (Fig. 6 and Table 4).

Asn95 is located in the follistatin domain I, which is thought to be the heparin-binding site [26]. The site occupancy and structure of N-linked oligosaccharides on Asn95 may affect the heparin-binding ability of FS. Heparin/heparan sulfate proteoglycans are known to exert an important influence on FS, which neutralizes the activity of activins. It is therefore possible that sialylated oligosaccharides at Asn95 control the activin-neutralizing activity via modulation of the heparin-binding ability of FS. In fact, it was reported that the N-glycosylation isoforms of antithrombin and heparin cofactor II differ substantially in their affinity for heparin [27,28]. We are currently studying the role played by oligosaccharides in the activin-neutralizing activity of FS; these studies employ the carbohydrate remodeling technique using the CHO cell line established in the present study.

Table 4
Putative structures of N-linked oligosaccharides deduced from the LC/MS of the glycopeptides corresponding to the Asn95 and Asn259

Carbohydrate Structure ^a	Asn95					Asn259				
	Ions in peak G1	Theoretical mass ^b	Observed <i>m/z</i> ^c			Ions in peak G2	Theoretical mass ^b	Observed <i>m/z</i>		
			M ²⁺	M ³⁺	M ⁴⁺			M ²⁺	M ³⁺	M ⁴⁺
	1	3216.2	-	1073.4	-	1	3958.1	-	1319.6	-
	2	3378.6	-	1126.6	-	2	4120.5	-	1373.9	-
	3	3669.6	1835.7	1223.2	-	3	4411.5	2206.3	1471.8	1104.7
	-	-	-	-	-	4	4427.5	2214.8	1475.7	-
	4	3960.9	-	1320.6	-	5	4702.8	-	1569.5	1177.1
	5	3976.6	-	1326.8	-	6	4718.8	-	1574.5	-
	6	3743.7	-	1248.6	-	7	4485.6	-	1497.2	-
	7	4034.9	2017.5	1346.9	-	-	-	-	-	-
	8	4326.2	-	1444.1	-	8	5068.1	-	-	1267.6

^a Proposed structures based on molecular weight. Symbols: solid squares, GlcNAc; open circles, mannose; open diamonds, galactose; dotted diamonds, fucose; solid circle, NeuAc; dotted circle, NeuGc.

^b Calculated average mass.

^c Mass of the ion measured in the positive-ion ESI mass spectrum from precursor-ion scan. Mass spectra were shown in Fig. 6.

Acknowledgements

We thank Dr. Y. Eto (Ajinomoto Co., Inc.) for providing the human FS315 cDNA. This work was supported by a grant-in-aid for the Research on Health Sciences Focusing on Drug Innovation from the Japan Health Sciences Foundation.

References

- [1] Robertson DM, Klein R, de Vos FL, McLachlan RI, Wettenhall RE, Hearn MT, et al. The isolation of polypeptides with FSH suppressing activity from bovine follicular fluid which are structurally different to inhibin. *Biochem Biophys Res Commun* 1987;149:744–9.
- [2] Ueno N, Ling N, Ying SY, Esch F, Shimasaki S, Guillemin R. Isolation and partial characterization of follistatin: a single-chain Mr 35,000 monomeric protein that inhibits the release of follicle-stimulating hormone. *Proc Natl Acad Sci USA* 1987;84:8282–6.
- [3] Nakamura T, Takio K, Eto Y, Shibai H, Titani K, Sugino H. Activin-binding protein from rat ovary is follistatin. *Science* 1990;247:836–8.
- [4] Kogawa K, Nakamura T, Sugino K, Takio K, Titani K, Sugino H. Activin-binding protein is present in pituitary. *Endocrinology* 1991;128:1434–40.
- [5] Massague J. The transforming growth factor-beta family. *Annu Rev Cell Biol* 1990;6:597–641.
- [6] Kingsley DM. The TGF-beta superfamily: new members, new receptors, and new genetic tests of function in different organisms. *Genes Dev* 1994;8:133–46.
- [7] Wada M, Shintani Y, Kosaka M, Sano T, Hizawa K, Saito S. Immunohistochemical localization of activin A and follistatin in human tissues. *Endocr J* 1996;43:375–85.
- [8] Sugino K, Kurosawa N, Nakamura T, Takio K, Shimasaki S, Ling N, et al. Molecular heterogeneity of follistatin, an activin-binding protein. Higher affinity of the carboxyl-terminal truncated forms for heparan sulfate proteoglycans on the ovarian granulosa cell. *J Biol Chem* 1993;268:15579–87.
- [9] Patel K. Follistatin. *Int J Biochem Cell Biol* 1998;30:1087–93.
- [10] Inouye S, Guo Y, DePaolo L, Shimonaka M, Ling N, Shimasaki S. Recombinant expression of human follistatin with 315 and 288 amino acids: chemical and biological comparison with native porcine follistatin. *Endocrinology* 1991;129:815–22.
- [11] Sumitomo S, Inouye S, Liu XJ, Ling N, Shimasaki S. The heparin binding site of follistatin is involved in its interaction with activin. *Biochem Biophys Res Commun* 1995;208:1–9.
- [12] Hashimoto O, Nakamura T, Shoji H, Shimasaki S, Hayashi Y, Sugino H. A novel role of follistatin, an activin-binding protein, in the inhibition of activin action in rat pituitary cells. Endocytotic degradation of activin and its acceleration by follistatin associated with cell-surface heparan sulfate. *J Biol Chem* 1997;272:13835–42.
- [13] Kobata A. Structures and functions of the sugar chains of glycoproteins. *Eur J Biochem* 1992;209:483–501.
- [14] Varki A. Biological roles of oligosaccharides: all of the theories are correct. *Glycobiology* 1993;3:97–130.
- [15] Itoh S, Kawasaki N, Ohta M, Hyuga M, Hyuga S, Hayakawa T. Study on evaluating methods for the quality control of glycoprotein products. (III)—Erythropoietin products. Part 3. *Bull Natl Inst Health Sci* 2001;65–9.
- [16] Simultaneous microanalysis of N-linked oligosaccharides in a glycoprotein using microbore graphitized carbon column liquid chromatography–mass spectrometry. *J Chromatogr A* 2002;968:89–100.
- [17] Kawasaki N, Ohta M, Hyuga S, Hashimoto O, Hayakawa T. Analysis of carbohydrate heterogeneity in a glycoprotein using liquid chromatography/mass spectrometry and liquid chromatography with tandem mass spectrometry. *Anal Biochem* 1999;269:297–303.
- [18] Kawasaki N, Ohta M, Hyuga S, Hyuga M, Hayakawa T. Application of liquid chromatography/mass spectrometry and liquid chromatography with tandem mass spectrometry to the analysis of the site-specific carbohydrate heterogeneity in erythropoietin. *Anal Biochem* 2000;285:82–91.
- [19] Kawasaki N, Haishima Y, Ohta M, Itoh S, Hyuga M, Hyuga S, et al. Structural analysis of sulfated N-linked oligosaccharides in erythropoietin. *Glycobiology* 2001;11:1043–9.
- [20] Kawasaki N, Ohta M, Itoh S, Hyuga M, Hyuga S, Hayakawa T. Usefulness of sugar mapping by liquid chromatography/mass spectrometry in comparability assessments of glycoprotein products. *Biologicals* 2002;30:113–23.
- [21] Ohta M, Kawasaki N, Hyuga S, Hyuga M, Hayakawa T. Selective glycopeptide mapping of erythropoietin by on-line high-performance liquid chromatography–electrospray ionization mass spectrometry. *J Chromatogr A* 2001;910:1–11.
- [22] Ohta M, Kawasaki N, Itoh S, Hayakawa T. Usefulness of glycopeptide mapping by liquid chromatography/mass spectrometry in comparability assessment of glycoprotein products. *Biologicals* 2002;30:235–44.
- [23] Hardy MR, Townsend RR, Lee YC. Monosaccharide analysis of glycoconjugates by anion exchange chromatography with pulsed amperometric detection. *Anal Biochem* 1988;170:54–62.
- [24] Kawasaki N, Ohta M, Hyuga S, Hyuga M, Hayakawa T. Application of liquid chromatography/mass spectrometry and liquid chromatography with tandem mass spectrometry to the analysis of the site-specific carbohydrate heterogeneity in erythropoietin. *Anal Biochem* 2000;285:82–91.
- [25] Ingrassia D, Fowler AV, Bleibaum J, Clarke S. Specificity of endoproteinase Asp-N (*Pseudomonas fragi*): cleavage at glutamyl residues in two proteins. *Biochem Biophys Res Commun* 1989;162:1528–34.
- [26] Inouye S, Ling N, Shimasaki S. Localization of the heparin binding site of follistatin. *Mol Cell Endocrinol* 1992;90:1–6.
- [27] Picard V, Ersdal-Badju E, Bock SC. Partial glycosylation of antithrombin III asparagine-135 is caused by the serine in the third position of its N-glycosylation consensus sequence and is responsible for production of the beta-antithrombin III isoform with enhanced heparin affinity. *Biochemistry* 1995;34:8433–40.
- [28] Bohme C, Nimtz M, Grabenhorst E, Conradt HS, Strathmann A, Ragg H. Tyrosine sulfation and N-glycosylation of human heparin cofactor II from plasma and recombinant Chinese hamster ovary cells and their effects on heparin binding. *Eur J Biochem* 2002;269:977–88.



Analysis of site-specific glycosylation in recombinant human follistatin expressed in Chinese hamster ovary cells

Masashi Hyuga*, Satsuki Itoh, Nana Kawasaki, Miyako Ohta,
Akiko Ishii, Sumiko Hyuga, Takao Hayakawa

Division of Biological Chemistry and Biologicals, National Institute of Health Sciences, 1-18-1, Kamiyoga, Setagaya-ku, Tokyo 158-8501, Japan

Received 22 October 2003; accepted 1 April 2004

Abstract

Follistatin (FS), a glycoprotein, plays an important role in cell growth and differentiation through the neutralization of the biological activities of activins. In this study, we analyzed the glycosylation of recombinant human FS (rhFS) produced in Chinese hamster ovary cells. The results of SDS-PAGE and MALDI-TOF MS revealed the presence of both non-glycosylated and glycosylated forms. FS contains two potential *N*-glycosylation sites, Asn95 and Asn259. Using mass spectrometric peptide/glycopeptide mapping and precursor-ion scanning, we found that both *N*-glycosylation sites were partially glycosylated. Monosaccharide composition analyses suggested the linkages of fucosylated bi- and triantennary complex-type oligosaccharides on rhFS. This finding was supported by mass spectrometric oligosaccharide profiling, in which the *m/z* values and elution times of some of the oligosaccharides from rhFS were in good agreement with those of standard oligosaccharides. Site-specific glycosylation was deduced on the basis of the mass spectra of the glycopeptides. It was suggested that biantennary oligosaccharides are major oligosaccharides located at both Asn95 and Asn259, whereas the triantennary structures are present mainly at Asn95.

© 2004 The International Association for Biologicals. Published by Elsevier Ltd. All rights reserved.

Abbreviations: CHO, Chinese hamster ovary; FCS, fetal calf serum; FS, follistatin; GCC, graphitized carbon column; GnT, *N*-acetylglucosaminyl-transferase; HPAEC-PAD, high-pH anion-exchange chromatography with pulsed amperometric detection; IEF, isoelectric focusing; LC/MS, liquid chromatography/mass spectrometry; MALDI-TOF MS, matrix-assisted laser desorption/ionization time-of-flight mass spectrometry; NeuAc, *N*-acetyl neuraminic acid; NeuGc, *N*-glucoryl neuraminic acid; PNGaseF, peptide *N*-glycanase F; rhFS, recombinant human follistatin; SDS-PAGE, sodium dodecyl sulfate-polyacrylamide gel electrophoresis; TFA, trifluoroacetic acid

1. Introduction

Follistatin (FS), a glycoprotein, was first discovered in ovarian follicular fluid as an inhibitor of pituitary follicle-stimulating hormone secretion [1,2]. Subsequent studies have revealed that FS can bind to activins and neutralize their biological activities [3,4]. Activins are members of the transforming growth factor- β superfamily, and they play important roles in the regulation of cell growth and in the differentiation processes that lead to morphogenesis in early vertebrate development [5,6]. Since FS and activins are broadly distributed,

they are not confined solely to tissues associated with reproduction [7].

FS is present in heterogeneous forms [8]. The FS gene consists of 315 amino acids, and it includes six exons (Fig. 1); alternative splicing can generate two isoforms, i.e. a 315-amino-acid protein (the full-length form, FS315) and a 288-amino-acid protein (the carboxy-truncated form, FS288) [9]. The activin-neutralizing activity of FS288 is higher than that of FS315 [10,11], which appears to correlate with their heparin/heparan sulfate proteoglycan-binding abilities [12]. The heterogeneity of FS is also due to diverse glycosylation. FS has two potential *N*-glycosylation sites (Asn95 and Asn259). Oligosaccharides are generally known to play important roles in defining the properties of glycoproteins such as their biological activity, immunogenicity,

* Corresponding author. Fax: +81-3-3700-9084.
E-mail address: mhyuga@nihs.go.jp (M. Hyuga).

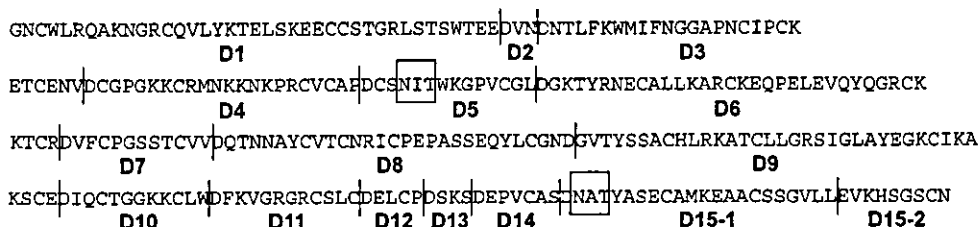


Fig. 1. Amino acid sequence of rhFS. Predicted cleavage sites with Asp-N are indicated by |. The potential *N*-glycosylation sites are indicated by boxes.

pharmacokinetics, solubility, and protease resistance [13,14]. Glycosylation on FS is also likely to exert an effect on activin-neutralizing activity; however, neither structure of the N-linked oligosaccharides in FS, nor their physiological roles, have been clarified due to the limited availability of these oligosaccharides.

The aim of this study was to elucidate the glycosylation of FS. We previously developed an oligosaccharide profiling method using liquid chromatography/mass spectrometry (LC/MS) equipped with a graphitized carbon column (GCC) [15–22]. Recently, we demonstrated a procedure for facilitating the structural analysis of glycoproteins [16]. Carbohydrate profiles and site-specific glycosylations can be characterized by the GCC-LC/MS method, followed by mass spectrometric peptide/glycopeptide mapping. We used this method to demonstrate here the carbohydrate heterogeneity and the site-specific N-linked oligosaccharide structures in recombinant human FS288 (rhFS) produced in Chinese hamster ovary (CHO) cells, in which a sufficient amount of FS could be expressed.

2. Materials and methods

2.1. Materials

Human FS315 cDNA and recombinant human activin A were kindly provided by Dr. Yuzuru Eto (Ajinomoto Co., Inc., Kawasaki, Japan). CHO cells were obtained from the Japanese Cancer Research Resources Bank (Tokyo, Japan). Mammalian expression vector pcDNA3.1/Hygro was purchased from Invitrogen (Carlsbad, CA, USA). LipofectAMINE plus reagent, Ham's F12 medium, fetal calf serum (FCS) and hygromycin were purchased from Life Technologies Inc. (Rockville, MD, USA). Pellicon XL membrane and Immobilon-P membrane were purchased from Millipore Corp. (Bedford, MA, USA). Sulfated-cellulofine was purchased from Seikagaku Corp. (Tokyo, Japan). Neuraminidase was purchased from Nakalai Tesque (Kyoto, Japan). *N*-glycosidase F (PNGaseF) and endo-proteinase Asp-N (Asp-N) were purchased from Boehringer Mannheim (Mannheim, Germany). All other chemicals were obtained from commercial sources and were of the highest purity available.

2.2. Establishment of a CHO cell line expressing rhFS

Complementary DNA encoding human FS288, was constructed from FS315 cDNA, and was cloned into pcDNA3.1/Hygro. This expression vector was transfected into CHO cells with LipofectAMINE plus reagent, according to the manufacturer's instructions. To screen the transformants, the transfectants were cultured with Ham's F12 medium supplemented with 10% FCS and 1 mg/ml hygromycin. After 2 weeks, the colonies were lifted with a micropipette. Expression levels of rhFS were assessed by an activin-neutralizing assay. The candidates were cloned by limiting dilution twice and were assessed again. The most productive rhFS-expressing clone (CHO-FS) was used in the following experiments.

2.3. Preparation of rhFS

Semi-confluent CHO-FS cells were cultured in Ham's F12 medium supplemented with 2% FCS. The conditioned medium was concentrated to a 1/10 volume by filtration with a Pellicon XL membrane (M_r 5000 cut), and was applied onto a sulfated-cellulofine column (2.5 × 20 cm) at 2 ml/min. The column was washed with 50 mM Tris-HCl (pH 8) containing 0.5 M NaCl, and the protein was eluted with 50 mM Tris-HCl (pH 8) containing 1.5 M NaCl. The effluent from the column was fractionated, and rhFS was monitored on Western blots using polyclonal anti-FS antibody. The fractions containing rhFS were injected into an HPLC (Hitachi D7000, Hitachi Co., Tokyo, Japan) apparatus equipped with a reversed-phase column (Vydac C4, 10 × 300 mm, The Separations Group, Inc., Hesperia, CA, USA). The protein was eluted with a linear gradient of 16–48% of acetonitrile/0.1% trifluoroacetic acid (TFA) for 30 min at a flow rate of 2 ml/min. Elution of proteins was monitored at 280 nm and individual peaks were manually collected. Fraction of rhFS was monitored on Western blots using polyclonal anti-FS antibody.

2.4. SDS-PAGE analysis of rhFS

RhFS was digested with or without PNGaseF at 37 °C for 24 h. The proteins were separated by sodium dodecyl sulfate-polyacrylamide gel electrophoresis

(SDS-PAGE) on 10% polyacrylamide gel. The gel was stained with Coomassie blue.

2.5. Isoelectric focusing

RhFS was dissolved in 100 mM ammonium acetate buffer, pH 4.5, and incubated with neuraminidase at 37 °C for 18 h. The proteins were precipitated with cold acetone and separated by isoelectric focusing (IEF). The gel was stained with Coomassie blue.

2.6. MALDI-TOF MS

RhFS (20 µg) was subjected to positive-ion matrix-assisted laser desorption/ionization time-of-flight mass spectrometry (MALDI-TOF MS), using a Shimadzu/KRATOS MALDI I instrument (Shimadzu Co., Kyoto, Japan) with 3,5-dimethoxy-4-hydroxy-cinnamic acid as the matrix.

2.7. Monosaccharide composition analysis

Monosaccharide composition analysis was performed according to the method reported by Hardy et al. [23]. Briefly, rhFS (50 µg) was hydrolyzed with 2 M TFA at 100 °C for 3 h. Monosaccharide compositions were analyzed by high-pH anion-exchange chromatography with pulsed amperometric detection (HPAEC-PAD) using a DX-300 system (Dionex, Sunnyvale, CA, USA) equipped with a CarboPac PA-1 anion exchange column (4 × 250 mm, Dionex).

2.8. Preparation of N-linked oligosaccharides alditols

N-linked oligosaccharides alditols were prepared by a previously described method [20]. Briefly, rhFS (100 µg) was digested with 5 units of PNGaseF at 37 °C for 2 days. Proteins were precipitated with 75% cold ethanol. The oligosaccharides were incubated with NaBH₄ at room temperature for 2 h. Excess reagent was decomposed with diluted acetic acid. The mixture was applied to a Supelclean ENVI-Carb column (Supelco, Bellefonte, PA, USA), which was washed with H₂O to remove the salts. Borohydride-reduced oligosaccharides were eluted with 30% acetonitrile/5 mM ammonium acetate.

2.9. Sugar profiling by LC/MS

Sugar profiling was carried out using a MAGIC 2002 system (Michrom BioResources, Inc., Auburn, CA, USA) connected to a TSQ7000 triple-stage quadrupole mass spectrometer (ThermoFinnigan, San Jose, CA, USA) in the positive-ion mode. The column used was a GCC (Hypercarb 5 µm, 1.0 × 150 mm, ThermoFinnigan). The eluents were 5 mM ammonium acetate (pH

9.6) containing 2% acetonitrile (pump A); and 5 mM ammonium acetate (pH 9.6) containing 80% acetonitrile (pump B). The N-linked oligosaccharide alditols were eluted at a flow rate of 50 µl/min for 80 min with a gradient of 5–30% in pump B. The ESI voltage was set at 4500 V, and the capillary temperature was 175 °C. The electron multiplier was set at 1200 V.

2.10. Asp-N digestion

RhFS was reduced and S-carboxymethylated as previously described [20]. Briefly, rhFS (100 µg) was dissolved in 0.5 M Tris-HCl buffer (pH 8.6) containing 8 M guanidine and 5 mM EDTA. After reduction with 2-mercaptoethanol at room temperature for 2 h, monoiodoacetic acid was added and incubated at room temperature for 2 h in the dark. Reduced and S-carboxymethylated-rhFS (equivalent to 100 µg of rhFS) was digested with Asp-N (2 µg) in 25 mM NH₄HCO₃ (pH 8.0) at 37 °C for 20 h. The predicted peptides to be obtained by Asp-N digestion were sequentially designated as D1–D15 (Fig. 1).

2.11. Peptide/glycopeptide mapping of Asp-N-digested rhFS

Peptide/glycopeptide mapping was carried out using a MAGIC 2002 system connected to a TSQ7000 triple-stage quadrupole mass spectrometer in the positive-ion mode. The column used was a MAGIC C18 column (1.0 × 150 mm, Michrom BioResources). The eluents were 2% acetonitrile/0.05% TFA (pump A), and 80% acetonitrile/0.05% TFA (pump B). Asp-N-digested rhFS was eluted with a linear gradient from 5 to 45% in pump B at a flow rate of 50 µl/min for 40 min. The eluate was monitored at 206 nm. The ESI voltage was set at 4500 V, and the capillary temperature was 175 °C. The electron multiplier was set at 1200 V. Precursor-ion scanning was performed using argon gas as the collision gas at a pressure of 2 mTorr. The collision energy was adjusted to –25 eV. The scan rate was 3 s/scan.

3. Results

3.1. Heterogeneity of rhFS

The carbohydrate heterogeneity of rhFS was analyzed by SDS-PAGE with and without PNGaseF digestion. The intact rhFS migrated as bands of an apparent molecular mass of 32 kDa and 33–36 kDa under non-reducing conditions (Fig. 2A, lane 1). PNGaseF digestion resulted in the disappearance of the multiple bands at 33–36 kDa with increases in the 32-kDa band (Fig. 2A, lane 2). These results suggest that the 32 kDa band and higher molecular weight bands are

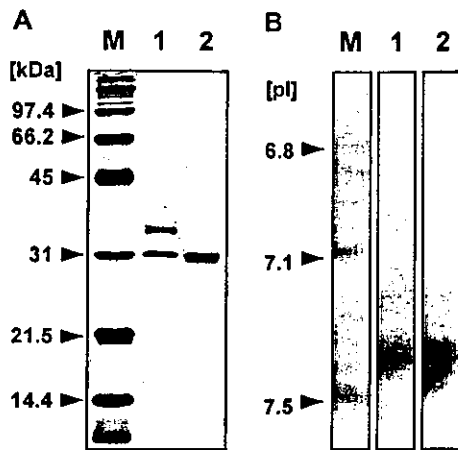


Fig. 2. (A) SDS-PAGE analysis of intact rhFS (lane 1) and PNGaseF-digested rhFS (lane 2). Lane M represents molecular weight markers. (B) IEF of intact rhFS (lane 1) and neuraminidase-digested rhFS (lane 2). Lane M represents pI markers.

the non-glycosylated FS and the glycosylated FS with diverse N-linked oligosaccharides, respectively.

The sialic acid heterogeneity of rhFS was analyzed by IEF with and without neuraminidase digestion. IEF of intact rhFS showed that the majority of the isoforms are located from pI 6.9 to 7.4 (Fig. 2B, lane 1). After treatment with neuraminidase, the acidic bands had disappeared and shifted at pI 7.4 (Fig. 2B, lane 2). These results suggested that the sialic acids contribute to the heterogeneity and the charge of rhFS.

The distribution of glycoforms was further investigated by MALDI-TOF MS. As shown in Fig. 3, multiple ions were detected in the range of 31.5–37 kDa. The most abundant ion at m/z 31,525 corresponded to the theoretical mass of non-glycosylated FS (31,514 Da). The other ions at m/z 33,804 and 35,600 could have

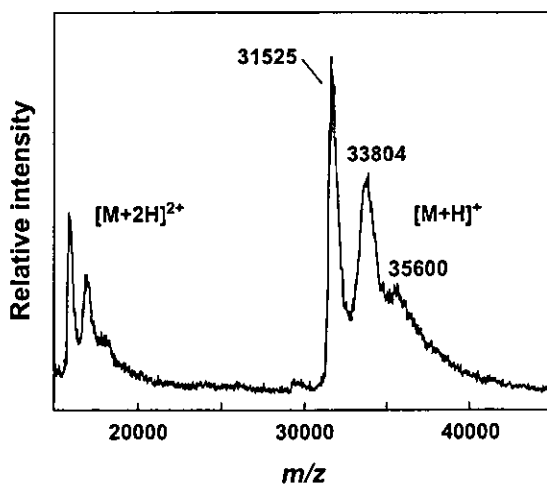


Fig. 3. MALDI-TOF MS analysis of intact rhFS. The peaks at m/z 31,525, 33,804 and 35,600 correspond to the non-glycosylated and glycosylated form of rhFS, respectively.

been monoglycosylated FS and diglycosylated FS, respectively.

3.2. Monosaccharide composition of rhFS

Monosaccharide composition was analyzed by hydrolysis followed by HPAEC-PAD. The relative molecular ratio of fucose and glucosamine were estimated at 1.2 and 4.4, respectively, when mannose was considered as 3.0 (Table 1). This result suggests the presence of fucosylated bi- and triantennary-type oligosaccharides. No galactosamine residue was detected, suggesting the absence of O-linked oligosaccharides.

3.3. N-linked oligosaccharides in rhFS

N-linked oligosaccharides were released from rhFS by PNGaseF digestion and reduced with NaBH₄ to avoid the separation of anomers. Then the oligosaccharide alditols from rhFS were analyzed by GCC-LC/MS. Fig. 4 shows the total ion current chromatogram of N-linked oligosaccharide alditols. The m/z values of intense ions observed in major peaks (peaks 8 and 12) were 1040.7²⁺ and 1186.4²⁺, which were consistent with the theoretical m/z values of [dHex][Hex]₅[HexNAc]₄[NeuAc]²⁺ and [dHex][Hex]₅[HexNAc]₄[NeuAc]₂²⁺, respectively (Table 2). The elution times of these oligosaccharides were in good agreement with those of fucosyl biantennary oligosaccharides bearing mono- and di-NeuAc prepared from erythropoietin, respectively [24]. An ion at m/z 1041.4²⁺ was also detected in peak 6. This oligosaccharide could be a sialylation isomer of peak 8 (1040.7²⁺).

Likewise, the ions at m/z 1790.7⁺ and 895.4²⁺ in peak 2 and at m/z 1077.9²⁺ in peak 3 were assigned as an asialo fucosylated biantennary oligosaccharide and an asialo fucosylated triantennary oligosaccharide, respectively. The ion at m/z 2389.6⁺ and 1194.6²⁺ in peak 11 was consistent with [dHex][Hex]₅[HexNAc]₄[NeuAc][NeuGc]²⁺ or [Hex]₆[HexNAc]₄[NeuAc]₂²⁺, respectively. The ions at m/z 2097.7⁺ and 1048.6²⁺ in peak 5 and at m/z 2096.5⁺ and 1049.5²⁺ in peak 8 were consistent with [dHex][Hex]₅[HexNAc]₄[NeuGc]²⁺ or [Hex]₆[HexNAc]₄[NeuAc]²⁺, respectively. The minor ions at m/z 1224.1²⁺, 1224.3²⁺, 1369.7²⁺, 1369.8²⁺,

Table 1
Monosaccharide composition analysis of rhFS oligosaccharides

Monosaccharide	Relative molar proportions ^a
Fucose	1.2
Galactosamine	0.3
Glucosamine	4.4
Galactose	3.2
Glucose	0.3
Mannose	3.0

^a Data are normalized to three-mannose residues.

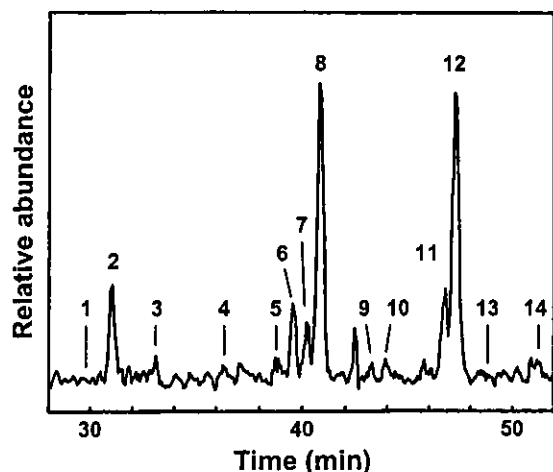


Fig. 4. Sugar map of oligosaccharide alditols released from rhFS. N-linked oligosaccharide alditols from rhFS were separated with GCC. The total ion content was scanned using the positive-ion mode at m/z 700–2400.

1370.5^{2+} and 1515.5^{2+} in peaks 7, 9, 11, 12, 13 and 14 were deduced to the fucosylated triantennary oligosaccharides with NeuAc, respectively.

The ratio of oligosaccharides was estimated as follows: fucosylated biantennary, ca. 85%, and fucosylated triantennary structures, ca. 10%, based on their ion currents; these results were in good agreement with the results of the monosaccharide composition analysis.

3.4. Site-specific glycosylation of rhFS

FS contains two potential *N*-glycosylation sites (Asn95 and Asn259, Fig. 1). The site-specific glycosylation and other post-translational modifications, such as phosphorylation and hydroxylation, were analyzed by mass spectrometric peptide/glycopeptide mapping (Fig. 5a, Table 3). Most of the non-glycosylated peptides were detected except for the small peptides, i.e. peptides D2 (tripeptide), D13 (tetrapeptide), and D12 (pentapeptide), which suggests the absence of *O*-glycans and any post-translational modifications on these peptides. The small peptides have no putative *N*-glycosylation site (Fig. 1), and no galactosamine residue was detected (Table 1). These findings suggest the absence of *N*- and *O*-linked oligosaccharides. However, the possibility remains that the small peptides are modified, such as by phosphorylation. Two unpredicted peptides (m/z 1176.2²⁺ and 510.4²⁺) were detected among the Asp-N digests of rhFS. They were assigned to peptides D15-1 and D15-2, which were produced from peptide D15 by further cleavage at the amino-terminal of Glu280. It was reported that a cleavage at the N-terminal site of glutamic acid is a possible cut site for Asp-N under the same conditions [25]. Peptides D5 and D15-1, each of which

Table 2
Putative structures of N-linked oligosaccharides deduced from the GCC-LC/MS

Peak No. ^a	Carbohydrate structure ^b	Theoretical mass ^c	Observed mass ^d		
			M ⁺	M ²⁺	M ³⁺
1		1627.5	1628.3	814.2	-
2		1789.7	1790.7	895.4	-
3		2155.0	-	1077.9	-
4		1934.7	-	967.9	-
5		2096.9	2097.7	1048.6	-
6		2080.9	2081.2	1041.4	-
7		2446.3	-	1224.1	817.4
8		2096.9	2096.5	1049.6	-
		2080.9	2082.2	1040.7	-
9		2446.3	-	1224.3	-
10		2226.0	-	1114.2	-
11		2388.2	2389.6	1194.6	-
		2737.5	-	1369.7	913.4
12		2372.2	2372.2	1186.4	-
		2737.5	-	1369.8	-
13		2737.5	-	1370.5	913.8
14		3028.8	-	1515.5	-

Note: The observed m/z of *1 and *2 are also consistent with the theoretical m/z value of $[\text{Hex}]_6[\text{HexNAc}]_4[\text{NeuAc}]$ and $[\text{Hex}]_6[\text{HexNAc}]_4[\text{NeuAc}]_2$, respectively.

^a Peak label in Fig. 4.

^b Proposed structures based on molecular weight. Symbols: solid squares, GlcNAc; open circles, mannose; open diamonds, galactose; dotted diamonds, fucose; solid circle, NeuAc; dotted circle, NeuGc.

^c Calculated average mass.

^d Mass of the ion measured in the positive-ion ESI mass spectrum from alditols.

have potential glycosylation site, were detected as non-glycosylated forms in the peptide/glycopeptide map.

Precursor-ion scanning, which can detect $[\text{Hex}][\text{HexNAc}]^+$ at m/z 366 produced by collision-induced dissociation, was performed for the monitoring of the glycopeptides. The TIC chromatogram of the precursor-ion scanning showed two significant peaks, peaks G1 and G2 (Fig. 5b). Fig. 6 shows the mass spectra of peaks G1 and G2 in Fig. 5b. On the basis of the theoretical masses of the peptides and oligosaccharides identified by sugar mapping (Table 2), peaks G1 and G2

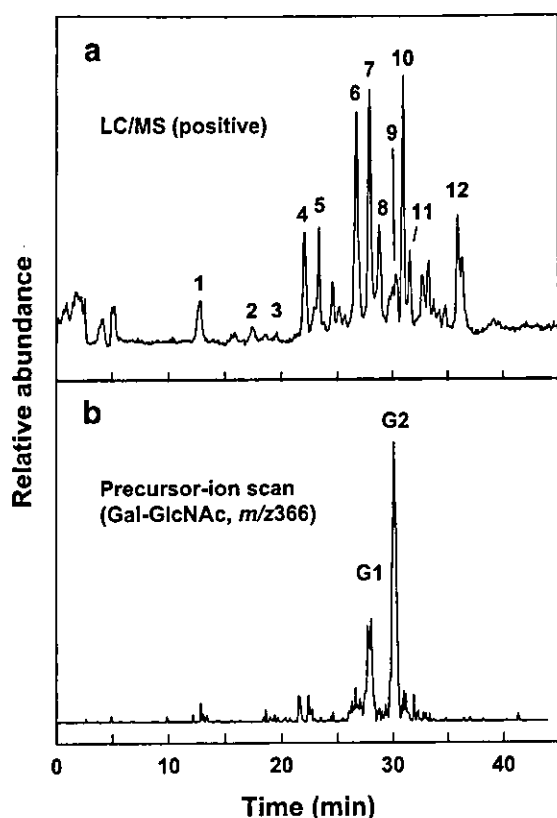


Fig. 5. Peptide/glycopeptide map of the rhFS Asp-N digest. The total ion current chromatogram of LC/MS in the positive-ion mode at m/z 400–2400 (a), and the TIC chromatogram of LC/MS/MS, precursor-ion scan of m/z 366 (b).

were assigned to glycosylated D5 and D15-1, respectively. The oligosaccharides attached to each *N*-glycosylation site were deduced as shown in Table 4. By comparing the *N*-linked oligosaccharide structures on

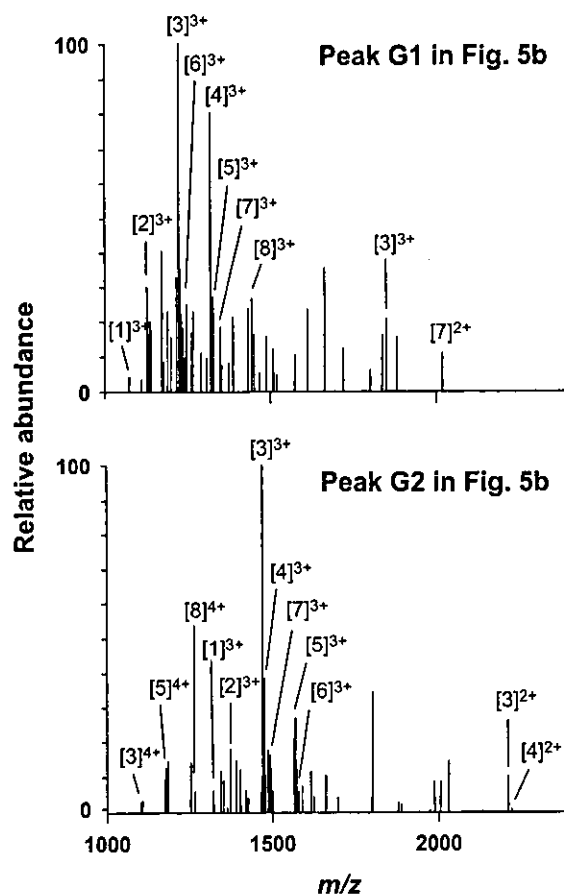


Fig. 6. Mass spectra of glycopeptides in peaks G1 and G2 in Fig. 5b. The observed m/z value of each ion is summarized in Table 4.

Asn95 with those on Asn259, it was concluded that biantennary oligosaccharides are major oligosaccharides located at both Asn95 and Asn259, whereas the triantennary structures are present mainly at Asn95.

Table 3
Assignment of the peaks in Fig. 5a

Peak no. ^a	Peptide ^b	Theoretical mass ^c	Observed m/z ^d					
			M^+	M^{2+}	M^{3+}	M^{4+}	M^{5+}	M^{6+}
1	D4	2666.0	—	1334.2	889.9	667.4	—	—
2	D14	777.8	778.6	—	—	—	—	—
3	D15-2 ^e	1018.0	1019.0	510.4	—	—	—	—
4	D11	1456.6	1457.5	729.0	486.3	—	—	—
5	D6	4378.8	—	—	1460.8	1095.5	—	—
6	D8	3326.4	—	1664.6	1109.5	—	—	—
	D10	1467.6	1468.2	734.8	490.1	—	—	—
7	D1	4728.1	—	—	1577.0	1183.2	947.0	789.6
8	D7	1329.4	1330.2	665.3	—	—	—	—
9	D5	1608.7	1609.3	805.1	—	—	—	—
10	D9	4165.6	—	—	1389.0	1042.2	834.1	—
11	D15-1 ^e	2350.6	—	1176.2	784.2	—	—	—
12	D3	3219.5	—	1610.1	1073.8	806.4	—	—

^a Peak label in Fig. 5a.

^b Predicted peptides were shown in Fig. 1.

^c Calculated average mass.

^d Mass of the ions measured in the positive-ion ESI mass spectrum from precursor-ion scan.

^e Peptide derived from D15 peptide.

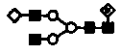
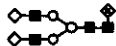
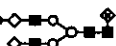
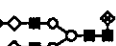
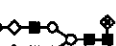
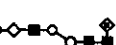



4. Discussion

The aim of the present study was to analyze the distribution of the glycoforms and the carbohydrate structures of rhFS. Previous study of FS isolated from porcine ovary has shown that porcine FS exists in six isoforms, due to alternative splicing and the site occupancy of N-linked oligosaccharides [8]. In this study, we used rhFS288 to eliminate the heterogeneity due to alternative splicing. The results of SDS-PAGE and MALDI-TOF MS revealed the presence of both non-glycosylated and glycosylated forms (Figs. 2 and 3). FS contains two potential N-glycosylation sites. Using mass spectrometric peptide/glycopeptide mapping and precursor-ion scanning, we found that both N-glycosylation sites were partially glycosylated (Fig. 5 and Table 3). Non-glycosylated and glycosylated proteins containing Asn95 and Asn259 were detected in the peptide/glycopeptide map and precursor-ion scanning, respectively. Monosaccharide composition analyses suggested the presence of linkages of fucosylated bi- and triantennary complex-type oligosaccharides on rhFS (Table 1). This finding was supported by mass spectrometric oligosaccharide profiling, in which the m/z values and

elution times of some of the oligosaccharides from rhFS were in good agreement with those of standard oligosaccharides. The site-specific glycosylations were deduced on the basis of the mass spectra of glycopeptides. It was suggested that biantennary oligosaccharides attach to both Asn95 and Asn259, whereas triantennary oligosaccharides attach mainly to Asn95 (Fig. 6 and Table 4).

Asn95 is located in the follistatin domain I, which is thought to be the heparin-binding site [26]. The site occupancy and structure of N-linked oligosaccharides on Asn95 may affect the heparin-binding ability of FS. Heparin/heparan sulfate proteoglycans are known to exert an important influence on FS, which neutralizes the activity of activins. It is therefore possible that sialylated oligosaccharides at Asn95 control the activin-neutralizing activity via modulation of the heparin-binding ability of FS. In fact, it was reported that the N-glycosylation isoforms of antithrombin and heparin cofactor II differ substantially in their affinity for heparin [27,28]. We are currently studying the role played by oligosaccharides in the activin-neutralizing activity of FS; these studies employ the carbohydrate remodeling technique using the CHO cell line established in the present study.

Table 4
Putative structures of N-linked oligosaccharides deduced from the LC/MS of the glycopeptides corresponding to the Asn95 and Asn259

Carbohydrate Structure ^a	Asn95					Asn259				
	Ions in peak G1	Theoretical mass ^b	Observed m/z ^c			Ions in peak G2	Theoretical mass ^b	Observed m/z		
			M ²⁺	M ³⁺	M ⁴⁺			M ²⁺	M ³⁺	M ⁴⁺
	1	3216.2	-	1073.4	-	1	3958.1	-	1319.6	-
	2	3378.6	-	1126.6	-	2	4120.5	-	1373.9	-
	3	3669.6	1835.7	1223.2	-	3	4411.5	2206.3	1471.8	1104.7
	-	-	-	-	-	4	4427.5	2214.8	1475.7	-
	4	3960.9	-	1320.6	-	5	4702.8	-	1569.5	1177.1
	5	3976.6	-	1326.8	-	6	4718.8	-	1574.5	-
	6	3743.7	-	1248.6	-	7	4485.6	-	1497.2	-
	7	4034.9	2017.5	1346.9	-	-	-	-	-	-
	8	4326.2	-	1444.1	-	8	5068.1	-	-	1267.6

^a Proposed structures based on molecular weight. Symbols: solid squares, GlcNAc; open circles, mannose; open diamonds, galactose; dotted diamonds, fucose; solid circle, NeuAc; dotted circle, NeuGc.

^b Calculated average mass.

^c Mass of the ion measured in the positive-ion ESI mass spectrum from precursor-ion scan. Mass spectra were shown in Fig. 6.

Acknowledgements

We thank Dr. Y. Eto (Ajinomoto Co., Inc.) for providing the human FS315 cDNA. This work was supported by a grant-in-aid for the Research on Health Sciences Focusing on Drug Innovation from the Japan Health Sciences Foundation.

References

- [1] Robertson DM, Klein R, de Vos FL, McLachlan RI, Wettenhall RE, Hearn MT, et al. The isolation of polypeptides with FSH suppressing activity from bovine follicular fluid which are structurally different to inhibin. *Biochem Biophys Res Commun* 1987;149:744–9.
- [2] Ueno N, Ling N, Ying SY, Esch F, Shimasaki S, Guillemin R. Isolation and partial characterization of follistatin: a single-chain Mr 35,000 monomeric protein that inhibits the release of follicle-stimulating hormone. *Proc Natl Acad Sci USA* 1987;84:8282–6.
- [3] Nakamura T, Takio K, Eto Y, Shibai H, Titani K, Sugino H. Activin-binding protein from rat ovary is follistatin. *Science* 1990;247:836–8.
- [4] Kogawa K, Nakamura T, Sugino K, Takio K, Titani K, Sugino H. Activin-binding protein is present in pituitary. *Endocrinology* 1991;128:1434–40.
- [5] Massague J. The transforming growth factor-beta family. *Annu Rev Cell Biol* 1990;6:597–641.
- [6] Kingsley DM. The TGF-beta superfamily: new members, new receptors, and new genetic tests of function in different organisms. *Genes Dev* 1994;8:133–46.
- [7] Wada M, Shintani Y, Kosaka M, Sano T, Hizawa K, Saito S. Immunohistochemical localization of activin A and follistatin in human tissues. *Endocr J* 1996;43:375–85.
- [8] Sugino K, Kurosawa N, Nakamura T, Takio K, Shimasaki S, Ling N, et al. Molecular heterogeneity of follistatin, an activin-binding protein. Higher affinity of the carboxyl-terminal truncated forms for heparan sulfate proteoglycans on the ovarian granulosa cell. *J Biol Chem* 1993;268:15579–87.
- [9] Patel K. Follistatin. *Int J Biochem Cell Biol* 1998;30:1087–93.
- [10] Inouye S, Guo Y, DePaolo L, Shimonaka M, Ling N, Shimasaki S. Recombinant expression of human follistatin with 315 and 288 amino acids: chemical and biological comparison with native porcine follistatin. *Endocrinology* 1991;129:815–22.
- [11] Sumitomo S, Inouye S, Liu XJ, Ling N, Shimasaki S. The heparin binding site of follistatin is involved in its interaction with activin. *Biochem Biophys Res Commun* 1995;208:1–9.
- [12] Hashimoto O, Nakamura T, Shoji H, Shimasaki S, Hayashi Y, Sugino H. A novel role of follistatin, an activin-binding protein, in the inhibition of activin action in rat pituitary cells. Endocytotic degradation of activin and its acceleration by follistatin associated with cell-surface heparan sulfate. *J Biol Chem* 1997;272:13835–42.
- [13] Kobata A. Structures and functions of the sugar chains of glycoproteins. *Eur J Biochem* 1992;209:483–501.
- [14] Varki A. Biological roles of oligosaccharides: all of the theories are correct. *Glycobiology* 1993;3:97–130.
- [15] Itoh S, Kawasaki N, Ohta M, Hyuga M, Hyuga S, Hayakawa T. Study on evaluating methods for the quality control of glycoprotein products. (III)—Erythropoietin products. Part 3. *Bull Natl Inst Health Sci* 2001;65–9.
- [16] Simultaneous microanalysis of N-linked oligosaccharides in a glycoprotein using microbore graphitized carbon column liquid chromatography–mass spectrometry. *J Chromatogr A* 2002;968:89–100.
- [17] Kawasaki N, Ohta M, Hyuga S, Hashimoto O, Hayakawa T. Analysis of carbohydrate heterogeneity in a glycoprotein using liquid chromatography/mass spectrometry and liquid chromatography with tandem mass spectrometry. *Anal Biochem* 1999;269:297–303.
- [18] Kawasaki N, Ohta M, Hyuga S, Hyuga M, Hayakawa T. Application of liquid chromatography/mass spectrometry and liquid chromatography with tandem mass spectrometry to the analysis of the site-specific carbohydrate heterogeneity in erythropoietin. *Anal Biochem* 2000;285:82–91.
- [19] Kawasaki N, Haishima Y, Ohta M, Itoh S, Hyuga M, Hyuga S, et al. Structural analysis of sulfated N-linked oligosaccharides in erythropoietin. *Glycobiology* 2001;11:1043–9.
- [20] Kawasaki N, Ohta M, Itoh S, Hyuga M, Hyuga S, Hayakawa T. Usefulness of sugar mapping by liquid chromatography/mass spectrometry in comparability assessments of glycoprotein products. *Biologicals* 2002;30:113–23.
- [21] Ohta M, Kawasaki N, Hyuga S, Hyuga M, Hayakawa T. Selective glycopeptide mapping of erythropoietin by on-line high-performance liquid chromatography–electrospray ionization mass spectrometry. *J Chromatogr A* 2001;910:1–11.
- [22] Ohta M, Kawasaki N, Itoh S, Hayakawa T. Usefulness of glycopeptide mapping by liquid chromatography/mass spectrometry in comparability assessment of glycoprotein products. *Biologicals* 2002;30:235–44.
- [23] Hardy MR, Townsend RR, Lee YC. Monosaccharide analysis of glycoconjugates by anion exchange chromatography with pulsed amperometric detection. *Anal Biochem* 1988;170:54–62.
- [24] Kawasaki N, Ohta M, Hyuga S, Hyuga M, Hayakawa T. Application of liquid chromatography/mass spectrometry and liquid chromatography with tandem mass spectrometry to the analysis of the site-specific carbohydrate heterogeneity in erythropoietin. *Anal Biochem* 2000;285:82–91.
- [25] Ingrosso D, Fowler AV, Bleibaum J, Clarke S. Specificity of endoproteinase Asp-N (*Pseudomonas fragi*): cleavage at glutamyl residues in two proteins. *Biochem Biophys Res Commun* 1989;162:1528–34.
- [26] Inouye S, Ling N, Shimasaki S. Localization of the heparin binding site of follistatin. *Mol Cell Endocrinol* 1992;90:1–6.
- [27] Picard V, Ersdal-Badju E, Bock SC. Partial glycosylation of antithrombin III asparagine-135 is caused by the serine in the third position of its N-glycosylation consensus sequence and is responsible for production of the beta-antithrombin III isoform with enhanced heparin affinity. *Biochemistry* 1995;34:8433–40.
- [28] Bohme C, Nimtz M, Grabenhorst E, Conradt HS, Strathmann A, Ragg H. Tyrosine sulfation and N-glycosylation of human heparin cofactor II from plasma and recombinant Chinese hamster ovary cells and their effects on heparin binding. *Eur J Biochem* 2002;269:977–88.

Enhancement of Hepatocyte Growth Factor-Induced Cell Scattering in *N*-Acetylglucosaminyltransferase III-transfected HepG2 Cells

Masashi HYUGA,* Sumiko HYUGA, Nana KAWASAKI, Miyako OHTA, Satsuki IROH, Shingo NIIMI, Toru KAWANISHI, and Takao HAYAKAWA

Division of Biological Chemistry and Biologicals, National Institute of Health Sciences; 1-18-1 Kamiyoga, Setagaya-ku, Tokyo 158-8501, Japan. Received January 9, 2004; accepted March 29, 2004; published online April 1, 2004

N-Acetylglucosaminyltransferase III (GnT-III), which catalyzes the synthesis of a bisecting GlcNAc residue of *N*-glycans, is thought to be involved in the function of glycoproteins such as growth factor receptors. We investigated the effects of the overexpression of GnT-III on the hepatocyte growth factor (HGF) receptor c-Met, a glycoprotein, in human hepatocarcinoma HepG2 cells. GnT-III activity was elevated about 250-fold in HepG2 cells stably transfected with the GnT-III gene, whereas no significant change in GnT-III activity was observed in mock transfectants. Cell scattering assay revealed that HGF-induced cell scattering was enhanced depending on the GnT-III activities in the GnT-III transfectants. Western blot analysis and E-PHA lectin blot analysis showed that the level of c-Met protein was the same in both transfectants; however, the bisecting GlcNAc residue on c-Met was detected only in the GnT-III transfectants. Although the peak level of c-Met phosphorylation was not different in both transfectants, the level of tyrosine phosphorylation of c-Met decreased more rapidly in the GnT-III transfectants than in the mock transfectants. Furthermore, HGF-induced extracellular-regulated kinase (ERK) phosphorylation was slightly higher in the GnT-III transfectants than in the mock transfectants. These results show that overexpression of GnT-III in HepG2 cells enhances HGF-induced cell scattering, which may result from, at least in part, enhancement of HGF-induced ERK phosphorylation.

Key words *N*-acetylglucosaminyltransferase III; cell scattering; hepatocyte growth factor; c-Met; extracellular-regulated kinase (ERK)

N-Acetylglucosaminyltransferase III (GnT-III; EC 2.4.1.144) is one of the glycosyltransferases and catalyzes the synthesis of a bisecting GlcNAc residue to the β -mannoside of the trimannose core in *N*-glycans.¹⁾ After introduction of the bisecting GlcNAc residue to the biantennary sugar chain, further processing and elongation of *N*-glycans by the other glycosyltransferases are suppressed,^{2–4)} resulting in alterations of structure with reduction of size. It seems that GnT-III may affect the functions of various glycoproteins. In this respect, it is noteworthy that the overexpression of GnT-III affects receptor tyrosine kinases such as the epidermal growth factor (EGF) and NGF receptor Trk, followed by the modulation of signal transductions.⁵⁾ EGF inhibits the growth of U373 MG glioma cells, while the overexpression of GnT-III causes the decreased binding of EGF to its receptor and then autophosphorylation of the receptor, resulting in the increase in the cell growth rate.⁶⁾ In contrast, the overexpression of GnT-III in HeLaS3 cells does not affect EGF receptor autophosphorylation, but enhances internalization of the receptors, resulting in the increase of the EGF-induced phosphorylation of extracellular-regulated kinase (ERK).⁷⁾ In PC 12 cells, nerve growth factor-stimulated Trk receptor autophosphorylation and signal transduction was disrupted by the overexpression of GnT-III.⁸⁾ This evidence suggests that GnT-III may also affect the other growth factors-induced signal transduction by the modulation of the function of their receptors in some ways.

Since the expression of GnT-III is associated with many physiological and pathological processes in the liver, including its regeneration⁹⁾ and hepatocarcinogenesis,¹⁰⁾ it is assumed that GnT-III is involved in the processes via the modulation of some glycoproteins such as the receptor of the hepatocyte growth factor (HGF), c-Met. In the present study, we investigated the effects of the overexpression of GnT-III

on the scattering of human hepatocarcinoma HepG2 cells, a defined HGF-induced biological response.

MATERIALS AND METHODS

Materials The recombinant human HGF was purchased from R&D systems (Minneapolis, MN, U.S.A.). The Dulbecco's modified Eagle's medium (DMEM), fetal calf serum (FCS), ampicillin, G418, Lipofectamine plus, and Opti-MEM were purchased from Life Technologies Inc. (Rockville, MD, U.S.A.). The human brain cDNA was purchased from Origene Technologies Inc. (Rockville, MD, U.S.A.). The mammalian expression vector pCI-neo was purchased from Promega (Madison, WI, U.S.A.). The protease inhibitors cocktail was purchased from Sigma Chemical Co (St. Louis, MO, U.S.A.). The PVDF membrane was purchased from Millipore Corporation (Bedford, MA, U.S.A.). Biotinylated E-PHA was purchased from Vector Laboratories (Burlingame, CA, U.S.A.). Protein G-immobilized magnetic beads (BioMag Protein G) were purchased from Polysciences, Inc. (Warrington, PA, U.S.A.). The anti-human c-Met antibody (C-23), anti-phospho-ERK antibody (E-4) and anti-ERK antibody (K-23) were purchased from Santa Cruz Biotechnology, Inc. (Santa Cruz, CA, U.S.A.). The monoclonal anti-phosphotyrosine antibody (PY20) was purchased from Transduction Laboratories (Lexington, KY, U.S.A.). The biotinylated anti-mouse IgG antibody, biotinylated anti-rabbit IgG antibody, peroxidase-conjugated rabbit anti-mouse IgG, and ECL chemiluminescence detection kit were purchased from Amersham-Pharmacia Biotech (Piscataway, NJ, U.S.A.). The vectastain ABC kit was purchased from Vector Laboratories (Burlingame, CA, U.S.A.). All other chemicals were obtained from commercial sources, and were of the highest purity available.

* To whom correspondence should be addressed. e-mail: mhyuga@nih.go.jp

Cell Culture Human hepatocarcinoma HepG2 cells were obtained from the Japanese Cancer Research Resources Bank (Tokyo, Japan). The HepG2 cells and GnT-III gene transfectants were cultured in DMEM supplemented with 10% FCS and 0.1 mg/ml of ampicillin under a humidified atmosphere of 95% air and 5% CO₂. Following incubation for 1 d with serum-free DMEM, the cells were incubated with 50 ng/ml of HGF in serum-free DMEM.

Expression Vector Construct, Gene Transfection, and Selection of Cells The human GnT-III cDNA was amplified by PCR using human brain cDNA as a template. The cDNA fragment containing the entire coding sequence was inserted into the pCI-neo *EcoR* I site and the final construct, pCI-GnT-III, was obtained. The pCI-neo is a mammalian expression vector which includes the cytomegalovirus enhancer/promoter and the G418-resistant gene. HepG2 cells were plated in a 6-cm plastic culture dish at a density of 1×10^6 cells/ml. After 24 h, the cells were washed twice with ice-cold phosphate-buffered saline (PBS), pH 7.2, and the medium was changed to serum-free Opti-MEM. The pCI-GnT-III vector or pCI-neo vector (20 μ g) was mixed with Lipofectamine plus, 100 μ l of which was added to the HepG2 cells. After 5 h incubation, the medium was changed to DMEM supplemented with 10% FCS. Stable transfectants were selected using 1 mg/ml G418.

GnT-III Activity The GnT-III activity was measured according to the methods described previously.¹¹⁾ Briefly, cell pellets were homogenized in ice-cold PBS containing protease inhibitors, and the supernatant was obtained after removal of the nucleus fraction by centrifugation for 20 min at 900 \times g. The GnT-III activity in the supernatant was assayed by high performance liquid chromatography methods using the fluorescence-labeled sugar chain (GlcNAc β -1, 2-Man α -1, 6-[GlcNAc β -1, 2-Man α -1, 3-] Man β -1, 4-GlcNAc β -1, 4-GlcNAc-pyridylamino) as a substrate. The substrate was prepared according to the method of Tokugawa *et al.*¹²⁾

Cell Scattering Assay The HepG2 cells were plated in a 6-cm plastic culture dish at a density of 5×10^4 cells/ml. The HepG2 cells were allowed to grow as discrete colonies for 2–3 d. The culture medium was then replaced with fresh DMEM medium containing 50 ng/ml HGF. After 24 h, the cells were observed under a phase contrast microscope.

Immunoprecipitation and Western Blot Analysis The cultured cells were washed twice with ice-cold PBS and disrupted in the lysis buffer (20 mM Tris, pH 7.2, 1% Triton X-100, 10% glycerol, 1 mM APMSF, 5 mM aprotinin, 1 mM sodium orthovanadate, 10 mM sodium fluoride, and 10 mM iodoacetamide). The protein concentrations were determined using a protein assay kit (Bio-Rad, CA, U.S.A.). The cell-free lysates (1 mg) were immunoprecipitated with the anti-human c-Met antibody and protein G-immobilized magnetic beads (BioMag Protein G). For Western blot analysis, whole cell lysates or immunoprecipitates were subjected to 6 or 10% sodium dodecyl sulfate–polyacrylamide gel electrophoresis (SDS-PAGE) under reducing conditions, and then transferred to a PVDF membrane. The blot was blocked with 1% bovine serum albumin (BSA) in Tris-buffered saline containing 0.1% Tween 20 (TBST). For the detection of c-Met, the blot was incubated with anti-human c-Met antibody, and biotinylated anti-rabbit IgG antibody. For the detection of the phosphorylated tyrosine residues of c-Met, the blot was incubated

with a monoclonal anti-phosphotyrosine antibody, and peroxidase-conjugated rabbit anti-mouse IgG. For the detection of phosphorylated ERK1/2, the blot was incubated with anti-ERK antibody, and biotinylated anti-mouse IgG antibody. Biotinylated antibody was detected using a Vectastain ABC-kit, and the blots were developed using the ECL chemiluminescence detection kit according to the manufacturer's instructions.

Lectin Blot Analysis Immunoprecipitated c-Met were subjected to 6% SDS-PAGE and transferred to PVDF membranes, as described above. The blot was blocked with 1% BSA in TBST and then incubated with 1 μ g/ml biotinylated erythroagglutinating phytohemagglutinin (E-PHA) in TBST for 1 h at room temperature. After washing with TBST, the lectin-reactive proteins were detected using a Vectastain ABC kit and the ECL chemiluminescence detection kit.

RESULTS

Establishment of HepG2 Cell Lines Stably Expressing GnT-III The GnT-III expression vector pCI-GnT-III was transfected into the HepG2 cells. The G418-resistant cells were screened as candidates of the GnT-III transfectants. Two randomly selected G418-resistant clones were evaluated for GnT-III activity. The clones expressing moderately and highly were designated HepG2-III_m and HepG2-III_h, respectively. A pCI-neo vector transfectant, designated as HepG2-mock, was also established as a negative control. The GnT-III activity in the HepG2-III_m and HepG2-III_h cells was significantly elevated about 20- and 250-fold, respectively, whereas the activity in the HepG2-mock cells did not differ significantly among the parental HepG2 cells (Table 1).

Enhancement of HGF-Induced Cell Scattering in GnT-III Transfectants To determine the effect of the overexpression of GnT-III on the HGF-induced cell scattering, the GnT-III transfectants and mock transfectants were examined. When the HepG2-mock cells were cultured, they showed a cobble-stone shape and had formed colonies of the cells (Fig. 1A). No significant difference in cell morphology of the GnT-III transfectants was observed (Figs. 1B, C). HepG2-mock cells scattered following cell-cell dissociation by the stimulation with HGF (Fig. 1D). The cell scattering of the GnT-III transfectants was more pronounced than the HepG2-mock cells; the enhancement of cell scattering was most pronounced in the HepG2-III_h cells that had a high GnT-III activity (Figs. 1E, F).

Analysis of c-Met of GnT-III Transfectants The expression levels of the c-Met protein in GnT-III transfectants were analyzed by Western blot analysis. No significant change of the level of c-Met was observed (Fig. 2). To analyze the alterations of the N-glycan structure on c-Met, E-

Table 1. Enzyme Activities of GnT-III in Mock- and GnT-III Transfected HepG2 Cells

Cell line	GnT-III activity [pmol/h/mg protein]
HepG2	79 \pm 30
HepG2-mock	149 \pm 50
HepG2-III _m	1400 \pm 260
HepG2-III _h	19600 \pm 1350

Data were mean \pm S.E. of three separate experiments.

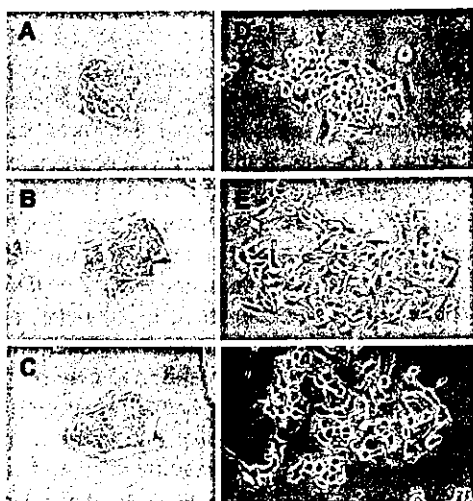


Fig. 1. HGF-Induced Cell Scattering in HepG2-Mock Cells and GnT-III Transfected HepG2 Cells

HepG2 mock-cells (A, D), HepG2-IIIh cells (B, E), and HepG2-IIIh cells (C, F) were cultured with (D, E, F) or without (A, B, C) HGF (50 ng/ml) for 24 h. Representative fields were photographed using a phase-contrast microscope.

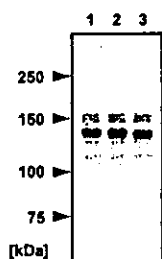


Fig. 2. Western Blot Analysis of c-Met

Total cell lysates from HepG2-mock cells (lane 1), HepG2-IIIh cells (lane 2), and HepG2-IIIh cells (lane 3) were subjected to 6% SDS-PAGE and then transferred to PVDF membrane. The blots were probed with anti-c-Met antibody.

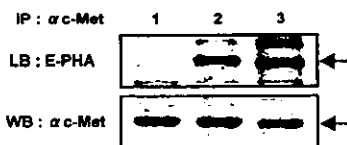


Fig. 3. Lectin Blot Analysis of c-Met

c-Met was immunoprecipitated from cell lysates of HepG2-mock cells (lane 1), HepG2-IIIh cells (lane 2), and HepG2-IIIh cells (lane 3). Immunoprecipitates were subjected to 6% SDS-PAGE and then transferred to PVDF membrane. The blots were probed with E-PHA (upper panel) or anti-c-Met antibody (lower panel). Arrows indicate c-Met.

PHA lectin blot analysis was performed. E-PHA binds specifically to bisecting GlcNAc residues.¹³⁾ Immunoprecipitated c-Met from the HepG2-IIIh cells and the HepG2-IIIh cells showed significant reactivity of E-PHA (Fig. 3), showing that *N*-glycan on c-Met was modified with bisecting GlcNAc residues. It was noted that the apparent molecular size of c-Met from the HepG2-IIIh cells were smaller than that from the HepG2-mock cells. The following experiments were performed with HepG2-IIIh cells and HepG2-mock cells.

Tyrosine Phosphorylation of c-Met in Gn T-III Transfectants To determine the effect of the GnT-III transfection on HGF signaling, HGF-induced tyrosine phosphorylation of

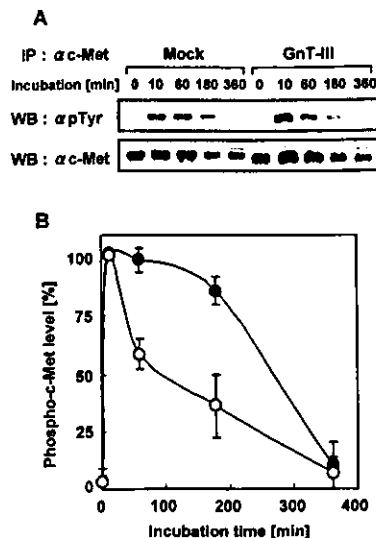


Fig. 4. The Time Course of the Tyrosine Phosphorylation of c-Met

(A) Cells were harvested at the indicated time after HGF treatment (50 ng/ml). c-Met, immunoprecipitated from the cell lysates of HepG2-mock cells (●) and HepG2-IIIh cells (○) were subjected to 6% SDS-PAGE and then transferred to a PVDF membrane. The blot was probed with anti-phosphotyrosine antibody (upper panel) or anti-human c-Met antibody (lower panel). One representative result of three separate experiments is shown. (B) The intensities of the bands obtained with phosphorylated c-Met were normalized to the intensities of the c-Met bands. These values are shown as percentages of the level of c-Met phosphorylation in HepG2-mock cells treated with HGF for 10 min (mean ± S.E., three separate experiments).

c-Met in HepG2-IIIh cells and HepG2-mock cells were examined. The c-Met phosphorylation level reached a peak by 10 min after the HGF treatment in each transfectant. Although no difference in the peak level of c-Met phosphorylation between the HepG2-IIIh cells and HepG2-mock cells was observed, the level of c-Met phosphorylation in the HepG2-IIIh cells was reduced more rapidly than in the HepG2-mock cells (Fig. 4).

ERK Activation in GnT-III Transfectants To further clarify the effect of the GnT-III transfection on HGF signaling, the HGF-induced phosphorylation of ERK in the HepG2-IIIh cells and HepG2-mock cells was also examined. The time course of the tyrosine phosphorylation of ERK showed that the phosphorylated ERK level reached a peak by 10 min after treatment in each transfectant. The peak level in the HepG2-IIIh cells was slightly higher than in the HepG2-mock cells (Fig. 5).

DISCUSSION

In this paper we investigated the effects of the overexpression of GnT-III on the scattering of human hepatocarcinoma HepG2 cells, a defined HGF-induced biological response, since the function of the HGF receptor c-Met could be modulated by GnT-III transfection followed by the alteration of its biological functions, as described in the "INTRODUCTION" section. The results showed that GnT-III gene transfection increases GnT-III activity by about 250 fold, followed by a significant increase of E-PHA reactivity with c-Met (Fig. 3), indicating that the transfection of GnT-III increased the amount of bisecting oligosaccharide residue on c-Met. In addition, the molecular size of c-Met in the HepG2-IIIh cells was smaller than that in the HepG2-mock cells (Figs. 2, 3), suggesting that an elongation of *N*-glycans on c-Met was

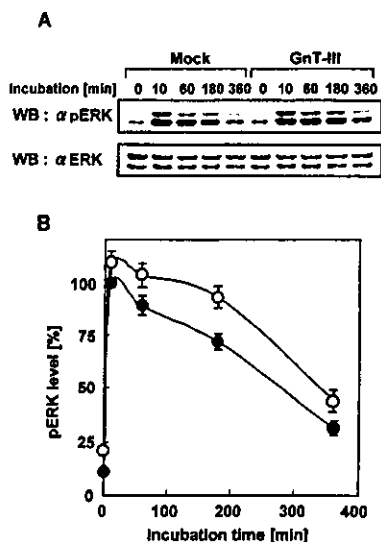


Fig. 5. The Time-Course of the Tyrosine Phosphorylation of ERK

(A) Cells were stimulated with 50 ng/ml HGF and harvested at the indicated times. Whole cell lysates of HepG2-mock cells (●) and HepG2-IIIh cells (○) were subjected to 10% SDS-PAGE and then transferred to a PVDF membrane. The blot was probed with anti-phospho-ERK antibody (upper panel) or anti-ERK antibody (lower panel). One representative result of three separate experiments is shown. (B) The intensities of the bands obtained with phospho-ERK were normalized to the intensities of the ERK bands. These values are shown as percentages of the level of ERK phosphorylation in HepG2-mock cells treated with HGF for 10 min (mean \pm S.E., three separate experiments).

suppressed by the bisecting GlcNAc residue. The same observation has been shown in various glycoproteins such as the EGF receptor,⁷ E-cadherin,^{14,15} and CD44.¹⁶

We investigated the effect of the overexpression of GnT-III on HGF-induced cell scattering using these transfectants, because cell scattering is one of the HGF-induced biological responses and an important component of several physiological and pathological processes. We found that HGF-induced cell scattering in the GnT-III transfectants was enhanced depending on the GnT-III activities. As far as we know, this is the first report of the enhancing effect of HGF-induced cell scattering by the overexpression of GnT-III.

To confirm the effect of GnT-III overexpression on HGF signaling, we first investigated the effect on the HGF-induced tyrosine phosphorylation of c-Met in GnT-III transfectants. Unexpectedly, the peak level of the tyrosine phosphorylation of c-Met did not change by GnT-III. In addition, the level of c-Met phosphorylation was reduced quite a bit more rapidly than that in the HepG2-mock cells. Previous studies shown that HGF stimulation also leads to down-regulation of the receptor.¹⁷ We assume that the rapid dephosphorylation was caused by up-regulated HGF signaling.

We further examined the effects on the HGF-induced phosphorylation of ERK, because ERK activation is associated with HGF-induced cell scattering.¹⁸ The ERK phosphorylation was slightly enhanced by the GnT-III overexpression, showing that the enhancement of cell scattering involves the up-regulation of the HGF-induced ERK phosphorylation. The mechanisms by which GnT-III overexpression affects ERK activation is now under investigation. It has been shown that GnT-III overexpression enhances the EGF-induced ERK phosphorylation in HeLaS3 cells by up-regulation of the internalization rate of the receptors.⁷ A possible mechanism by which GnT-III overexpression enhances HGF-in-

duced ERK phosphorylation is that GnT-III affects c-Met internalization.

In this study, we demonstrated that GnT-III overexpression increased the amount of bisecting oligosaccharide structures and shortened the *N*-glycans associated with c-Met. Lectin blot analysis of total showed that *N*-glycans of the other glycoproteins were also changed by GnT-III overexpression (data not shown). Therefore, the glycoproteins involved in cell scattering, such as E-cadherin and integrin, are candidate proteins for involvement in the enhancement of cell scattering by GnT-III overexpression. In fact, it has been reported that GnT-III overexpression affects their biological functions.^{14,15,19} Further study is needed to clarify the mechanism involved in the enhancement of cell scattering.

In evaluating the significance of the present results, it seems worthwhile to examine the relation of the change of GnT-III with the action of HGF *in vivo*. In the normal rat liver, GnT-III activity is very low. However, the activity increased about 4-fold in regenerating rat liver.⁹ HGF is induced in regenerating rat liver, and stimulates hepatocyte growth. In addition, it was shown that hepatocarcinoma exhibited a high level of GnT-III activity, whereas normal liver contains very little.²⁰ Autocrine HGF signaling leads to abnormal malignant progression.²¹ Therefore, the increase of GnT-III may contribute to liver regeneration and hepatocarcinoma progression by the enhanced HGF signal.

In conclusion, we demonstrated that the overexpression of GnT-III caused the enhancement of HGF-induced cell scattering, and suggest that the enhancement of cell scattering involves, at least in part, enhancement of the HGF-induced ERK phosphorylation.

Acknowledgments This work was supported by a grant-in-aid for research on health sciences focusing on drug innovation from the Japan Health Sciences Foundation.

REFERENCES

- 1) Nishikawa A., Ihara Y., Hatakeyama M., Kangawa K., Taniguchi N., *J. Biol. Chem.*, **267**, 18199–18204 (1992).
- 2) Easton E. W., Bolscher J. G., van den Eijnden D. H., *J. Biol. Chem.*, **266**, 21674–21680 (1991).
- 3) Gu J., Nishikawa A., Tsuruoka N., Ohno M., Yamaguchi N., Kangawa K., Taniguchi N., *J. Biochem. (Tokyo)*, **113**, 614–619 (1993).
- 4) Sasai K., Ikeda Y., Eguchi H., Tsuda T., Honke K., Taniguchi N., *FEBS Lett.*, **522**, 151–155 (2002).
- 5) Stanley P., *Biochim. Biophys. Acta*, **1573**, 363–368 (2002).
- 6) Rebbaa A., Yamamoto H., Saito T., Meuillet E., Kim P., Kersey D. S., Bremer E. G., Taniguchi N., Moskal J. R., *J. Biol. Chem.*, **272**, 9275–9279 (1997).
- 7) Sato Y., Takahashi M., Shibukawa Y., Jain S. K., Hamaoka R., Miyagawa J., Yaginuma Y., Honke K., Ishikawa M., Taniguchi N., *J. Biol. Chem.*, **276**, 11956–11962 (2001).
- 8) Ihara Y., Sakamoto Y., Mihara M., Shimizu K., Taniguchi N., *J. Biol. Chem.*, **272**, 9629–9634 (1997).
- 9) Miyoshi E., Ihara Y., Nishikawa A., Saito H., Uozumi N., Hayashi N., Fusamoto H., Kamada T., Taniguchi N., *Hepatology*, **22**, 1847–1855 (1995).
- 10) Miyoshi E., Nishikawa A., Ihara Y., Gu J., Sugiyama T., Hayashi N., Fusamoto H., Kamada T., Taniguchi N., *Cancer Res.*, **53**, 3899–3902 (1993).
- 11) Nishikawa A., Fujii S., Sugiyama T., Taniguchi N., *Anal. Biochem.*, **170**, 349–354 (1988).
- 12) Tokugawa K., Oguri S., Takeuchi M., *Glycoconj. J.*, **13**, 53–56 (1996).
- 13) Yamashita K., Hitoi A., Kobata A., *J. Biol. Chem.*, **258**, 14753–14755

- (1983).
- 14) Yoshimura M., Ihara Y., Matsuzawa Y., Taniguchi N., *J. Biol. Chem.*, **271**, 13811—13815 (1996).
- 15) Kitada T., Miyoshi E., Noda K., Higashiyama S., Ihara H., Matsuura N., Hayashi N., Kawata S., Matsuzawa Y., Taniguchi N., *J. Biol. Chem.*, **276**, 475—480 (2001).
- 16) Sheng Y., Yoshimura M., Inoue S., Oritani K., Nishiura T., Yoshida H., Ogawa M., Okajima Y., Matsuzawa Y., Taniguchi N., *Int. J. Cancer*, **73**, 850—858 (1997).
- 17) Hammond D. E., Carter S., McCullough J., Urbe S., Vande Woude G., Clague M. J., *Mol. Biol. Cell.*, **14**, 1346—1354 (2001).
- 18) Sipeki S., Bander E., Buday L., Farkas G., Bacsy E., Ways D. K., Farago A., *Cell Signal*, **11**, 885—890 (1999).
- 19) Isaji T., Gu J., Nishiuchi R., Zhao Y., Takahashi M., Miyoshi E., Honke K., Sekiguchi K., Taniguchi N., *J. Biol. Chem.*, in press (2004).
- 20) Nishikawa A., Fujii S., Sugiyama T., Hayashi N., Taniguchi N., *Biochem. Biophys. Res. Commun.*, **152**, 107—112 (1988).
- 21) Vande Woude G. F., Jeffers M., Cortner J., Alvord G., Tsarfaty I., Resau J., *Ciba Found. Symp.*, **212**, 119—130; discussion 130—112, 148—154 (1997).

Kinetic Analysis of Pepsin Digestion of Chicken Egg White Ovomuroid and Allergenic Potential of Pepsin Fragments

Kayoko Takagi^a Reiko Teshima^a Haruyo Okunuki^a Satsuki Itoh^a
Nana Kawasaki^a Toru Kawanishi^a Takao Hayakawa^a Yoichi Kohno^b
Atsuo Urisu^c Jun-ichi Sawada^a

^aNational Institute of Health Sciences, Tokyo; ^bDepartment of Pediatrics, Graduate School of Medicine, Chiba University, Chiba, and ^cDepartment of Pediatrics, Fujita Health University School of Medicine, Aichi, Japan

Key Words

Ovomucoid · Allergen · Digestion · Simulated gastric fluid · Fragment, pepsin-digested · Human serum IgE

Abstract

Background: The allergenic potential of chicken egg white ovomucoid (OVM) is thought to depend on its stability to heat treatment and digestion. Pepsin-digested fragments have been speculated to continue to exert an allergenic potential. OVM was digested in simulated gastric fluid (SGF) to examine the reactivity of the resulting fragments to IgE in sera from allergic patients. **Methods:** OVM was digested in SGF and subjected to SDS-PAGE. The detected fragments were then subjected to N-terminal sequencing and liquid chromatography/mass spectrometry/mass spectrometry analysis to confirm the cleavage sites and partial amino acid sequences. The reactivity of the fragments to IgE antibodies in serum samples from patients allergic to egg white was then determined using Western blotting ($n = 24$). **Results:** The rate of OVM digestion depended on the pepsin/OVM ratio in the SGF. OVM was first cleaved near the end of the first domain, and the resulting fragments were then further digested into smaller fragments. In the Western blot analysis, 93% of the OVM-reactive sera also bound to the 23.5- to 28.5-kDa fragments, and 21% reacted with

the smaller 7- and 4.5-kDa fragments. **Conclusion:** When the digestion of OVM in SGF was kinetically analyzed, 21% of the examined patients retained their IgE-binding capacity to the small 4.5-kDa fragment. Patients with a positive reaction to this small peptide fragment were thought to be unlikely to outgrow their egg white allergy. The combination of SGF-digestibility studies and human IgE-binding experiments seems to be useful for the elucidation and diagnosis of the allergenic potential of OVM.

Copyright © 2005 S. Karger AG, Basel

Introduction

Chicken egg white is one of the strongest and most frequent causes of food allergies among young children [1–5]. Egg white contains several allergens, including ovalbumin, ovomucoid, lysozyme and ovomucoid (Gal d 1, OVM). OVM accounts for about 11% of all egg white proteins [6] and has a molecular weight of 28 kDa, containing a carbohydrate content of 20–25% [7]. OVM is known to be stable to digestion and heat, and cooked eggs can cause allergic reactions in OVM-specific allergic patients [8–11]. One possible reason for this is that OVM contains linear epitopes that are only slightly affected by conformational changes induced by heat denaturation.

KARGER

Fax +41 61 306 12 34
E-Mail karger@karger.ch
www.karger.com

© 2005 S. Karger AG, Basel
1018-2438/05/1361-0023\$22.00/0

Accessible online at:
www.karger.com/iaa

Correspondence to: Dr. Reiko Teshima
National Institute of Health Sciences, Division of Biochemistry and Immunochemistry
1-18-1 Kamiyoga, Setagaya-ku
Tokyo 158-8501 (Japan)
Tel. +81 3 3700 1141, ext. 243, Fax +81 3 3707 6950, E-Mail rteshima@nihs.go.jp

OVM consists of 186 amino acids divided into three domains of about 60 amino acids each; the third domain has been reported to be the most important domain with regard to allergenicity [12]. In a previous report, N-glycans in the third domain were suggested to be essential for allergenicity [13]; however, a recent report found that the deletion of the N-glycans did not affect the allergic reactivity.

We previously reported the digestibility of 10 kinds of food proteins in simulated gastric fluid (SGF) [8, 14]. OVM was digested relatively rapidly, but several fragments were detected by sodium dodecyl sulfate-polyacrylamide gel electrophoresis (SDS-PAGE) followed by Coomassie blue (CBB) staining. The reactivity of these fragments with IgE antibodies from the sera of patients with egg white allergy is very important to understanding the mechanism of OVM allergy.

A few previous reports have described the reactivity of IgE in sera from patients with egg white allergies with OVM-derived fragments. Kovacs-Nolan et al. [15] separated pepsin-digested fragments of OVM using high-performance liquid chromatography (HPLC) and examined the IgE-binding activities of each fragment using an enzyme-linked immunosorbent assay (ELISA). Besler et al. [16] investigated the reactivity of pepsin-digested fragments with patient IgE using Western blotting and showed that the fragments retain their binding capacity to human IgE in some serum samples from OVM-allergic patients. However, little attention has been paid to the digestive conditions, and the number of serum samples has been somewhat small in these studies. Urisu et al. [17] reported that the sera of subjects that tested positive or negative during an oral egg white challenge exhibited a significant difference in their reactivity with pepsin fragments.

In the present report, kinetic data for different generations of SGF-stable OVM fragments were obtained, and the reactivity of the fragments with serum IgE from patients with egg white allergies was investigated using Western blotting.

Materials and Methods

Pepsin (catalog number P6887) and chicken egg white OVM (T2011, Trypsin Inhibitor, Type III-O) were purchased from Sigma Chemical Co. (St. Louis, Mo., USA). The concentration of the OVM test solution was 5 mg/ml of water. The gels and reagents used for the SDS-PAGE analysis were purchased from Invitrogen (Carlsbad, Calif., USA).

Serum Specimens

Sera from 24 patients with egg white allergies and a healthy volunteer were used after obtaining informed consent from the patients and ethical approval by the Institutional Review Board of the National Institute of Health Sciences. Twenty-two of the patients had been diagnosed as having an egg white allergy at hospitals in Japan, based on their clinical histories and positive IgE responses to egg white proteins by radioallergosorbent test (RAST), while the remaining 2 allergen-specific sera were purchased from Plasma Lab International (Everett, Wash., USA); the commercial sera originated from adult Caucasians who had been diagnosed as having several food allergies, including egg white, based on their clinical history and skin tests. The commercial sera also showed positive IgE responses to egg white proteins when examined using RAST.

Preparation of SGF

Pepsin (3.8 mg; approximately 13,148 units of activity) was dissolved in 5 ml of gastric control solution (G-con; 2 mg/ml NaCl, pH adjusted to 2.0 with distilled HCl), and the activity of each newly prepared SGF solution was defined as the production of a ΔA_{280} of 0.001/min at pH 2.0 and 37 °C, measured as the production of trichloroacetic acid-soluble products using hemoglobin as a substrate. The original SGF was prepared at a pepsin/OVM concentration of 10 unit/ μ g, and this solution was diluted with G-con for the experiments performed at pepsin/OVM concentrations of 1 and 0.1 unit/ μ g. The SGF solutions were used within the same day.

Digestion in SGF

SGF (1,520 μ l) was incubated at 37 °C for 2 min before the addition of 80 μ l of OVM solution (5 mg/ml). The digestion was started by the addition of OVM. At each scheduled time point (0.5, 2, 5, 10, 20, 30, and 60 min), 200 μ l of the reaction mixture was transferred to a sampling tube containing 70 μ l of 5 \times Laemmli buffer (40% glycerol, 5% 2-mercaptoethanol, 10% SDS, 0.33 M Tris, 0.05% bromophenol blue, pH 6.8) and 70 μ l of 200 mM Na₂CO₃. For the zero-point samples, the OVM solution (10 μ l) was added to neutralized SGF (190 μ l of SGF, 70 μ l of 5 \times Laemmli buffer, and 70 μ l of 200 mM Na₂CO₃). All neutralized samples were then boiled at 100 °C for 3 min and subjected to SDS-PAGE.

SDS-PAGE Analysis and Staining Procedure

Samples (15 μ l/lane) were loaded onto a 10–20% polyacrylamide Tris/Tricine gel (Invitrogen, Carlsbad, Calif., USA) and separated electrophoretically. The gels were fixed for 5 min in 5% trichloroacetic acid, washed for 2 h with SDS Wash (45.5% methanol, 9% acetic acid), stained for 10 min with CBB solution (0.1% Coomassie Brilliant blue R, 15% methanol, 10% acetic acid), and destained with 25% methanol and 7.5% acetic acid. The stained gel images were then analyzed using Image Gauge V3.1 (Fuji Film, Tokyo, Japan), and the density of each band was quantified. Periodic acid-Schiff (PAS) staining [18] was used to detect the glycosylated fragments.

N-Terminal Sequence Analysis

OVM (1.5 mg) was digested in SGF containing 1 unit/ml pepsin, concentrated by centrifugation using Centriprep YM-3 (Millipore Corporation, Bedford, Mass., USA) and subjected to SDS-PAGE followed by electrical transblotting to a 0.2- μ m polyvinylidene difluoride membrane (Bio-Rad, Richmond, Calif., USA) and CBB staining. The detected fragment bands were then cut out and sequenced using a Procise 494HT Protein Sequencing System (Applied Biosys-